Plant Water Management Experiments: Hydroponics 3 & 4

Marc B. Wasserman[1]
Portland State University, Portland, OR, 97201

Mark M. Weislogel[2] and Logan J. Torres[3]
IRPI LLC, Wilsonville, OR, 97070

Tyler R. Hatch[4] and John B. McQuillen[5]
NASA Glenn Research Center, Cleveland, OH, 44135

As humans consider longer-duration missions in space, NASA has identified production of fresh vegetables aboard spacecraft as beneficial for crew nutrition, mental wellbeing, and enabling bioregenerative life support (i.e., air, water, and waste processing). Current low-g plant growth techniques have successfully grown a variety of leafy and flowering plants. However, unique microgravity fluidics challenges to maintain plant moisture levels persist which hamper overall system reliability. The Plant Water Management (PWM) experiments seek to demonstrate low-cost, low-mass, reusable plant growth systems that leverage recent advances in low-g capillary fluidics phenomena to provide routine, largely passive, water delivery to plants. This paper presents findings from a series of PWM-Hydroponics 3 & 4 experiments, which were collected during three ISS flight operations that occurred in March, May, and July of 2021. Open hydroponic capillary channel flows with synthetic evapo-transpiring plant models were used. Tests demonstrated flow stability for single and parallel channel flow configurations across a range of flow rates, plant types, and plant arrangements. Technology demonstrations of both passive aeration and bubble phase separation are reported. We provide details of the data reduction and archive. Insights from the successful flight demonstrations provide a foundation from which follow-on PWM-Hydroponics 5 & 6 experiments on ISS, potentially incorporate living plants, are being considered.

Nomenclature

a	=	acceleration field strength (m/s^2)	MWA	=	Maintenance Work Area
f	=	dimensionless interface curvature function	PWM	=	Plant Water Management
F_i	=	dimensionless flow resistance coefficient ($\approx 1/7$)	α	=	interior corner half-angle
F_A	=	dimensionless corner flow area function	δ	=	surface curvature half-angle
H_i	=	meniscus centerline elevation at location I	μ	=	dynamic viscosity
L	=	length	θ	=	contact angle
L_p	=	pinning edge length	ρ	=	density
Q	=	volumetric flow rate	σ	=	surface tension

I. Introduction and Theory

As sketched in Figure 1, inertial-visco-capillary flows in open wedge channels have received significant research attention due to their routine occurrence in nature and industry.[1,2] For sufficiently wetting fluids in the absence of significant gravity, as fluid enters the channel at left and is withdrawn at right (see Figure 1), the elevation of the surface reduces along its length L and produces an increasingly negative capillary pressure that drives the fluid passively from left to right along the channel. Such flows are observed and exploited in many situations such as wicking flows within porous media and across hemi-porous surfaces. It can be shown that the impact of gravity and

[1] Graduate Student, Mechanical and Materials Engineering, 1930 SW 4th Ave.
[2] Principal Investigator, 27501 SW 95th Ave., Ste 930.
[3] Design Engineer, 27501 SW 95th Ave., Ste 930.
[4] Research Aerospace Engineer, NASA Glenn Research Center, 21000 Brookpark Rd
[5] Senior Research Aerospace Engineer, NASA Glenn Research Center, 21000 Brookpark Rd

other background accelerations a are negligible provided $\rho a L H_1 \tan\alpha/\sigma << 1$, where ρ is the density difference across the free surface, H_1 is the characteristic height of the liquid in the wedge, α is the wedge half-angle, and σ is the fluid surface tension. This constraint is met on earth when the length scales of the system H_1 and L are typically sub-millimetric.

Adopting the notation of Figure 1, the steady volumetric visco-capillary flow rate along the channel may be written

$$Q = \frac{\sigma}{\mu}\frac{H_1^3 F_A}{3L}\frac{F_i \sin^2\alpha}{f}\left(1 - \frac{H_2^3}{H_1^3}\right), \qquad \text{with} \qquad F_A = f^2\left(\frac{\cos\theta \sin\delta}{\sin\alpha} - \delta\right) \qquad \text{and} \qquad f = \frac{\sin\alpha}{\cos\theta - \sin\alpha}, \tag{1}$$

where $F_i \approx 1/7$ is a numerical flow resistant coefficient, μ is the fluid dynamic viscosity, H_1 and H_2 are the upstream and downstream meniscus heights respectively, and the dimensionless area and interface curvature functions are F_A and f, respectively with $\delta \equiv \pi/2 - \alpha - \theta$ as described in Ref. 3. It is of interest to observe that $Q \sim H_1^3$ such that in microgravity environments, where H_1 readily assumes values 100-fold those on earth, Q readily assumes values 10^6-fold those on earth. Such large, no-moving-parts flows are attractive for a variety of spacecraft applications including passive hydroponic plant watering systems for advanced research and food production in space. Large length scale wedge flows have been studied aboard the International Space Station (ISS) as part of the Capillary Flow Experiments (CFE)[4], Capillary Channel Flow (CCF)[5], and Capillary Structures for Exploration Life Support (CSELS)[6] experiments. The present work seeks to apply the state of the art to the challenging practical problems of microgravity hydroponics, which involve the single and two-phase bubbly evapotranspirational flow of contaminated liquids in poorly wetting channels with widely varying channel geometries dominated by unique microgravity plant root configurations. Solid models and sections of the 'Wedge' and 'Cylinder' hydroponics channels of PWM-Hydroponics 3 & 4 are provided in Figure 2 with critical dimensions noted.

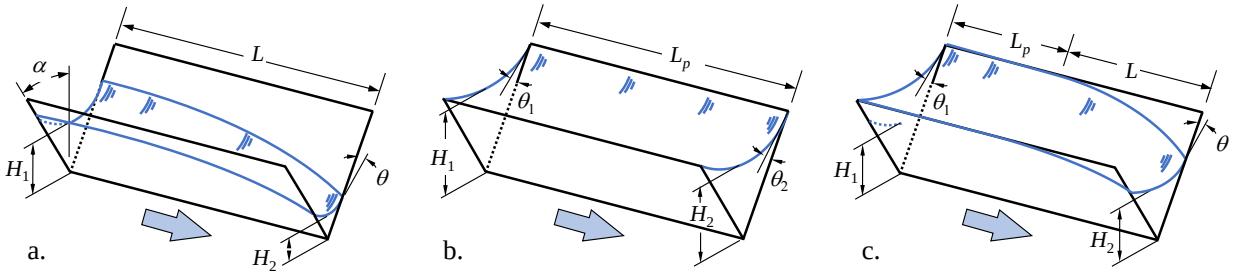

Figure 1. Open wedge channel capillary flow with a. free (L), b. pinned (L_p), and partially pinned contact line boundary conditions. Flow is introduced at left, removed at right, with capillary driven flow in between driven by cross flow free surface curvature gradient.

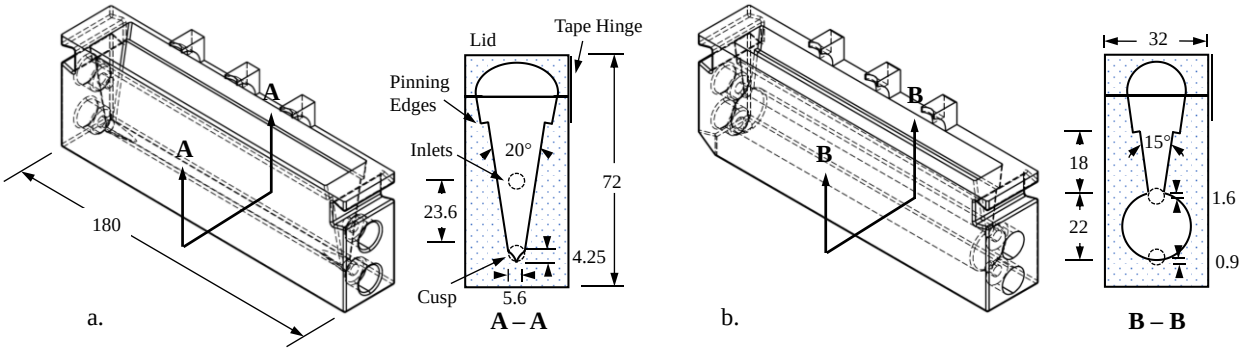

Figure 2. Open a. Wedge (76 mL) and b. Cylinder (79 mL) channels with sectional views employed by PWM-Hydroponics 3 & 4 on ISS. Approximate volumes to pinning edges provided. Inlets are sized for 1/4 in Luer Lock threaded fittings with 3/16 in ID tubing. All dimensions in mm. Active channel length is 150 mm.

II. PWM-Hydroponics Technology Demonstration

The Plant Water Management Hydroponics (PWM-Hydroponics) experiment is pursued by NASA as a series of low-cost, fast-to-flight technology demonstrations to show the feasibility of the general approach and to advance the

readiness level of the hydroponics technology. A background for the PWM experiments is provided in part in References 7 and 8. In this paper we focus on the PWM-Hydroponics 3 & 4 experiments operated on ISS over 6 approximately 8-hour crew days from March to July 2021. The central objectives of the demonstrations concern system priming, start-up, stable single and two-channel parallel flow, impact of single and multiple simple wicking and evapotranspiring plant models varying size and complexity, response to varying fill levels, flow rates, ease of plant insertion and removal, shut down, and more. Specific tests to identify the limits of stable operation as well as the passive mitigation, diversion, and separation of aerating bubbles were also pursued and reported in part herein. Over 400 individual tests were performed, the majority of which are only summarized. A reduced data archive with hyperlinked clips of the individual test set-points and video events will be made publicly available on the NASA PSI database (https://psi.nasa.gov). In this paper we provide a brief overview of the PWM-Hydroponics 3 & 4 hardware, ISS operations, data reduction, archive, and discussion of the salient preliminary results. We summarize the successes of the technology demonstrations with plans for follow-on demonstrations for PWM 5 & 6 currently in work.

III. PWM-Hydroponics 3 & 4 Experiment Overview

The PWM-Hydroponics hardware is designed for safety and simplicity of use. At the beginning of each operation, the hardware is manually unstowed and assembled on the portable Maintenance Work Area (MWA, i.e., workbench) aboard the International Space Station (ISS). All tests are performed by crew in the open cabin of the ISS, after which the assembly can be quickly drained, disassembled, and stowed, with all quantitative measures recorded via a single HD video camera (e.g., flow rate, fill levels, interface configurations, bubble distribution and velocity, etc.).

A. Test Stand and Test Cells

An image of the experimental set-up is provided in Figure 3. As identified on the figure, the hardware consists of two hydroponic test channels, a tubing harness that permits selectable flow to a single, serial, or parallel configuration, and a peristaltic pump to circulate liquid through the system. The test channels, fluid reservoir, and wye fittings are 3D printed Accura 60® parts and the 3/16" ID Tygon® tubing is connected using Luer Lock fittings. Two 60 mL syringes, labeled 'upstream' and 'downstream' by their position relative to the pump, are used to prime the system, to adjust liquid levels during operations, and to make up for liquid lost to wicking into or evaporation through the plant 'foliage.' A third 20 mL gas syringe is filled with cabin air and used to inject bubbles into the system during specific tests. The liquid for the tests is an in-flight re-constituted sugar-based tropical fruit punch prepared by the crew prior to the tests. The properties of the sweetened fruit drink are similar to typical plant nutrient solutions with surface tension $\sigma \approx 0.064$ N/m, density $\rho \approx 1010$ kg/m^3, dynamic viscosity $\mu = 0.0012$ kg/m·s, and channel polymer contact angle $\theta \approx 40 \pm 22°$ The variable-speed peristaltic pump provides flow in the range of 0.8-4.9 mL/s (for 3/16" ID pump head tubing). The pump flow delivery rate is nominally manually adjusted using the dial on the pump, with precise values determined post-flight from the image processing of the video footage via FFT analysis of the pump head rotation rate (we apply 0.857 mL/cycle for the 3/16" ID pump head tubing employed).[9] All components are mounted to an ULTEM™ 3D printed back and base plate, which is then secured to the MWA with hook-and-loop fasteners.

The hardware establishes a variety of flow configurations through the channels during operations. The channels are positioned (upper and lower) for simultaneous distortion-free observation of the flow behavior when operating in parallel flow mode. By configuring the polypropylene pinch valves, forward and reverse flows may be achieved in the single upper and lower channel paths, parallel upper and lower channel paths, and serial upper to lower channel paths using the serial bypass line. In all examples shown, the flow direction is left to right through the channels as pictured in Figure 3. The fluid reservoir was opened or closed to the flow path, passively adding make-up liquid to the system when open. The wye fittings identified in Figure 3a were interchanged with two pairs of bubble phase-separator fittings for demonstration of passive bubble phase separation just upstream of the channels.

Four copies each of two different hydroponic channel designs, or eight total channels, were tested. Channel perspective and sections with dimensions are provided in Figure 2. The Wedge channel type includes a 20° ($\alpha = 10°$) wedge with a 4.25 mm high cusp along the vertex. To be discussed in greater detail, the channel employs two parallel 90° pinning edges located 44.3 mm from the bottom edge for a maximum fluid volume of ~76 mL when filled to this height. The lower inlet for the Wedge channel is aligned with the bottom of the cusp and the upper inlet is 23.6 mm higher. The Cylinder channel type contains a 22 mm diameter cylindrical section in the lower portion of the channel, intended to provide additional room for plant roots. At the top of the cylinder, the channel transitions to a 15° wedge profile that continues for 18 mm before reaching the two parallel 90° pinning edges. When filled to this edge, the approximate volume of the Cylinder channel is 79 mL. The lower inlet for the Cylinder channel extends 0.9 mm below the lower edge of the cylindrical section and the upper inlet is centered 1.6 mm below the top edge of the same. Both

test cells include a curved lid with three slots for plant stem alignment. The lids are secured with clear tape which serves as a hinge when placing and removing plants, and for clearing the lid of liquid during stability tests.

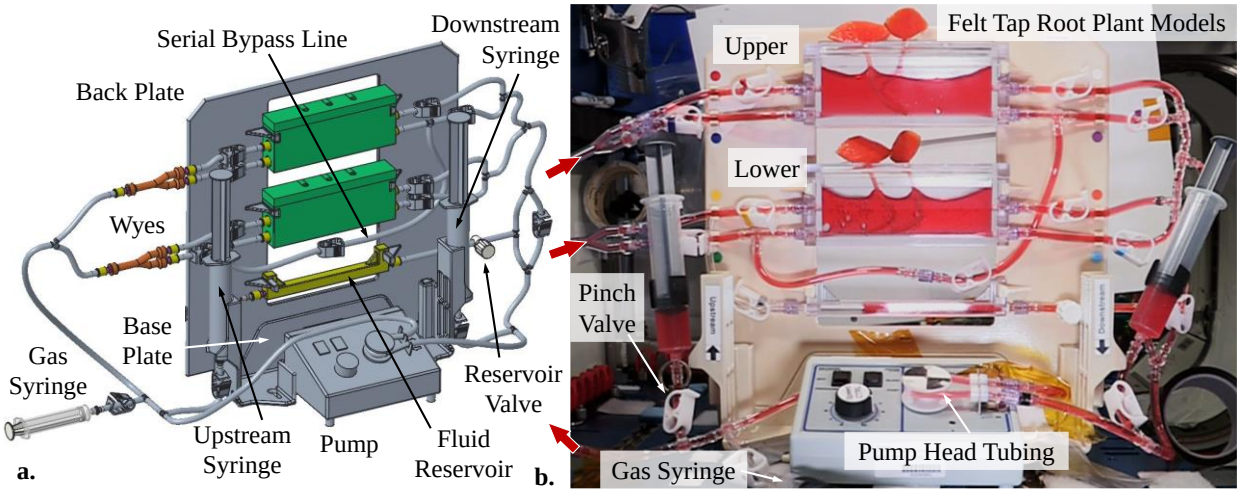

Figure 3. a. Solid model of PWM-Hydroponics hardware with b. image during flight operations (*Q* = 0-4.4 mL/s, parallel wedge channel flow, 2ea felt tap root models, clip refs. #59-63). The wye fittings are swappable for 3D printed gas/liquid phase separators and the test channels are swappable between Wedge and Cylinder styles. Plant models are readily added and removed. Upstream tubing is out of frame left in b.

Figure 4. Scaled images of the six plant models: a. Simulated Plant Kit with b. small (4ea), c. medium (4ea), and d. large synthetic weave (4ea), e. braided nylon (6ea), f. small (4ea), and g. large felt tap root (2ea). Dimensions in mm.

B. Plant Models

The PWM Hydroponics Simulated Plant Kit includes six different plant models based loosely on different root structures of terrestrial plants. Images of these models are provided in Figure 4. The Rayon felt models and foliage are 4 mm thick. The 80 μm OD fiber modacrylic synthetic hair weave models are cut to short (75 mm), medium (110 mm) and long (150 mm) lengths. The braided yellow nylon string models consist of 4 each 3-strand frayed lengths of 120, 100, 70, and 50 mm. The strands are made of 40 μm nylon fibers. All plant model roots pass through 25 mm long 4 mm ID coated shrink wrap just below the foliage. The shrink wrap acts as a non-wetting stem to support the foliage. A total of ten different plant configurations were demonstrated with up to three plants per channel. Though far from realistic, the plant models do serve the purposes of the PWM-Hydroponics demonstration by providing

wetting, wicking, and evapotranspiring 'devices' that also occlude the hydroponic channels to various degrees as might be expected of living plants.

C. ISS Experiment Operations

Flight operations for the PWM-Hydroponics 3 & 4 demonstrations were conducted by six crew members in three test series: March 30-31, May 26-27, and July 27-28, 2021. Two pairs each of Wedge and Cylinder channels were sent to the ISS. The first experiment series included both Wedge and Cylinder channels, the second series focused only on Wedge channels and the third series examined only Cylinder channels. Due to the possibility of microbial growth, current ISS safety protocols require the trashing of all wetted components after 48 hours of exposure. This requirement guided the decisions on the chronological order of tests performed regarding channel and plant model selection. ISS flight operations are summarized in Table 1. Each of the three runs included a hardware setup, system prime, experiment operations, complete teardown, and stow activity. During system prime and experiment operations, the investigator team had direct audio communication with the crew and real-time downlink video from a Sony Camcorder with 1280x720 pixel resolution at either 30 or 60 fps. The crew also took still images throughout the demonstrations using a Nikon D5 DSLR camera. The crew downlinked the locally recorded HD video and still images to the ground after each operation.

Table 1. Summary of 2021 PWM-Hydroponics 3 & 4 operations, for Wedge (W) and Cylinder (C) channels.

GMT Day	Date (m/d)	Channel (W/C)	Select Demonstrations	Crew Time (hh:mm)
89	3/30	W	Single/parallel flow rate sweeps, plants	6:00
90	3/31	W/C	Flows with plants, gas bubble injections, flows at multiple fill levels w/ plants	7:50
146	5/26	W	Flows with plants, parallel long-duration runs, serial flow demo, passive fluid reservoir demo	9:15*
147	5/27	W	Gas bubble injections, parallel long-duration runs, phase separator/bubble diverter demo	7:50
208	7/27	C	Flows with plants, parallel long-duration runs, passive fluid reservoir demo	8:00
109	7/28	C	Flows with plants, parallel long-duration runs	7:50

**Includes setup time during previous afternoon*

D. Data Reduction

In total, the PWM-Hydroponics 3 & 4 experiments produced slightly over 39 hours of video footage. To support subsequent analyses, the footage is catalogued in over 430 clips of the various demonstrations and test-points. Each clip is annotated with the date, NASA operation name (OpNom), astronaut name, flow configuration, flow rate, plant models used, and a brief qualitative description of the clip contents. A summary table highlighting different flow configurations performed and selected clips demonstrating these flows is shown in Table **2**.

The choice to demarcate each clip is somewhat subjective, however actions such as changing the flow rate, changing the flow configuration (i.e., single to parallel flow), changing the type, number, and order of the plant models, etc. are typical examples of actions used to demarcate clips. In case alternate clip splitting is desired in the future, each entry in the PWM 3 & 4 clips archive contains hyperlinks to both the clip and the original source file. As a note, audio was not always captured in the locally recorded video or may be captured but unintelligible. In these cases, space-to-ground communications are spliced into the downlinked video files and synchronized to the videos.

Whenever the pump head is visible within the video clip, the system flow rate is calculated by measuring the pump head rotation rate (Hz) and multiplying by the linear pump calibration 0.857 mL/cycle for the 3/16" ID pump head tubing set. For each test, 10 seconds of video is converted to still images. The pump head rotation rate is found by tracking the pixel intensity at a location on the pump head with time, as shown in Figure 5. Illustration of image data reduction process to determine pump flow rate: (left to right) still frame image of pump head, *z*-profile plot of pump head pixel intensity, and FFT with the pump-head frequency (in Hz) highlighted.

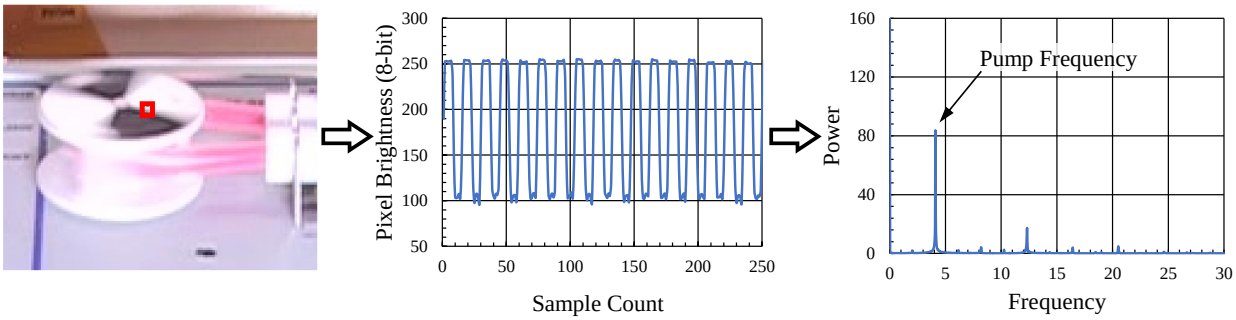

Figure 5. Illustration of image data reduction process to determine pump flow rate: (left to right) still frame image of pump head, *z*-profile plot of pump head pixel intensity, and FFT with the pump-head frequency (in Hz) highlighted.

Table 2. Overview of PWM-Hydroponics 3 & 4 operations. Clips are referenced to PWM 3 & 4 archive (https://psi.nasa.gov). Total experiment times for Wedge and Cylinder channels are 22:05 and 17:03, respectively.

Flow Demonstration	No. of Clips	Tot. Time (hh:mm)	Selected Clip Ref. Numbers
Wedge Channel Prime	10	1:38	2-4, 202-206, 265-266
Cylinder Channel Prime	4	0:58	142, 170, 384-385
Single Wedge Flows	234	12:34	1-19, 36-54, 63-102, 111-137, 204-218, 226-259, 265-289, 304-313, 316-354, 360-377
Single Cylinder Flows	72	4:43	144-198, 387-388, 431-436
Parallel Wedge Flows	61	7:07	20-35, 55-62, 103-110, 217-225, 290-300, 356-359
Parallel Cylinder Flows	30	9:21	389-391, 399-430
Serial Channel Flow	4	1:32	221-224
Gas Bubble Injections	129	7:04	64-67, 87-90, 96-100, 159-169, 270-289, 306-354
Wedge Flows with Plants	151	9:56	35-131, 226-261, 360-379
Cylinder Flows with Plants	86	13:01	152-195, 395-436
Bubble Diverter (Y or Teardrop)	142	8:31	141-200, 301-382
Passive Reservoir Drains	8	1:13	253-259, 396 (partial)
System Drains	34	4:52	69, 121, 138,197-198, 242, 261

To find the instantaneous liquid volume within a given channel, still images are extracted from the video clip of interest at a desired sampling rate (i.e., frames per second). The resulting image stack is thresholded, and several points (typically 30-50) are sampled across the top edge of the binary image to create a series of coordinates corresponding to the location of the free surface. These values are combined with the known shape of the Wedge or Cylindrical channels to find the fluid cross-sectional area at each location. The array is then integrated numerically using the trapezoidal rule to produce an approximate volume to within ± 5% (worst case), more typically ± 3% for most fill levels. The process is iterated for each image extracted from the video clip establishing the channel volume over time. Due to the resolution of the video files and significant contact angle hysteresis (~20° < θ < ~70°), we assume a flat fluid surface in the cross-flow direction. The impact of this assumption is accommodated within the estimated uncertainty of the measurement.

IV. Primary Preliminary Results

A. System Prime

At the beginning of each day's operations, the channels were primed with fluid using the upstream and downstream syringes. To prime the channel, an iterative approach was used where, using the downstream syringe, fluid is first dispensed from the righthand side only towards the center. Once the fluid reaches the approximate center of the channel, the process is repeated from the left using the upstream syringe until the two advancing fronts meet and merge to form a continuous surface across the channel. From this point, either syringe can be used to add additional liquid until the desired fill level is achieved. Figure 6 illustrates the stages of priming for the Wedge (a.-e.) and Cylinder (f.-j.) channels. In the figure, the first three stages of filling show the prime process simultaneously from both sides, however these images have been composited together for clarity. Chronologically, the right half of each channel was primed first followed by the left half in Figure 6a.-c. (and f.-h.), then the two halves merge in d. (i.), with a final fill level adjustment shown in Figure 6e (j.).

Due to contact angle hysteresis, inlet shape, and channel geometry, when filling from the lower inlets, the initial liquid introduced into the Wedge channel tends to spread in a fan-like shape both upwards and across the channel. The pinning edge does act as a barrier to prevent continued upward flow, however the limits of this barrier were not tested here. Instead, a pulsed infill technique, proposed by crewmember Kate Rubins during early operations, was found to be a simple and effective way to limit vertical spread, encourage axial fluid advance and reduce reliance on the pinning edge. The pulsed infill method involves cycling between adding and removing liquid from the channel. As shown in Figure 6a, liquid is initially added until the meniscus reaches the pinning edge. Fluid is then withdrawn from the channel in b., which reduces the height of the meniscus without affecting its axial position. When fluid is now added back to the channel, the shape of the meniscus and channel geometry encourages the fluid front to advance across the channel, as seen in Figure 6c.

During Cylinder channel priming, the pulsed infill technique was also utilized, however the geometry of the channel produces differences in the priming behavior. While the transition from cylindrical to wedge cross sections within the channel provides an additional pinning edge that promotes axial advance during priming (ref. Figure 2b for geometry), the shape also provides a rivulet destabilizing geometry that can lead to break-up of portions of liquid during the infill as shown in Figure 6f. When the channel prime on the right side began, the initial injection of fluid jetted a short distance before wetting the container, causing the fluid accumulation to be connected to the inlet by only a small rivulet along the bottom edge of the container. Another behavior seen in Figure 6i., to be discussed further in connection with Figure 8c, is the tendency of the meniscus to form a hemispherical depression as the liquid level drops below the cylinder-wedge transition. This geometry encourages gas bubble accumulation within the cylindrical portion of the channel.

Once initially wetted, both channels were readily re-primed when draining was required for plant installation during operations. As will be discussed further, a bubble-free prime was also found to not be critical because both channels are tolerant of small gas bubbles in the flow. While both channels also theoretically provide for passive bubble separation, the Wedge channel was found to be more robust in this capacity. This feature of the Wedge channel is explored more in Figure 13.

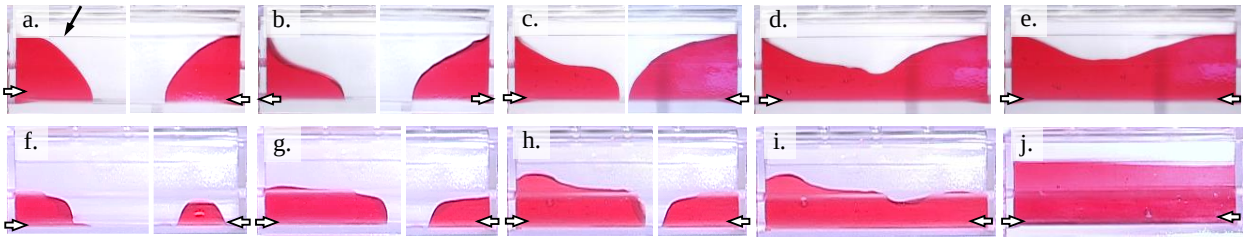

Figure 6. Sequential/iterative images of pulsed priming for Wedge (a.-e., GMT 89, clip ref. 3) and Cylinder (f.-j., GMT 90, clip ref. 142) channels. Black arrow in a. identifies pinning edge, white arrows identify fill/drain location and direction.

B. Stable Single Channel Flows

The low-g free surface stability of capillary flows in open wedge channels is well established in Refs. 3-6. The stability of such flows in the presence of plant models as obstacles is not. Figure 7 provides an example of the stability of single Wedge channel flow without plant model(s). At least 306 single channels 'runs' were completed, 184 with

plants, requiring 11:24 hrs of testing, with 6 tests held for over 10 min duration. The approximately 23 min demonstration (clip 2) in Figure 7 confirms an essentially constant channel volume to within ± 1% which is below measurement uncertainty of ± 3%, despite a near quadrupling of flow rate during the run. Figure 7b overlays the free surface height of four selected flow rates over a scaled image of the channel from the run presented in a. For the highest flow rate tested (4.77 mL/s), an approximately 3 mm increase in the height of the contact line is seen in the right third of the channel along with a decrease in meniscus height in the entrance region caused by the fast-moving flow. The contact line is otherwise stable to approximately 1 mm across the flow rate sweep.

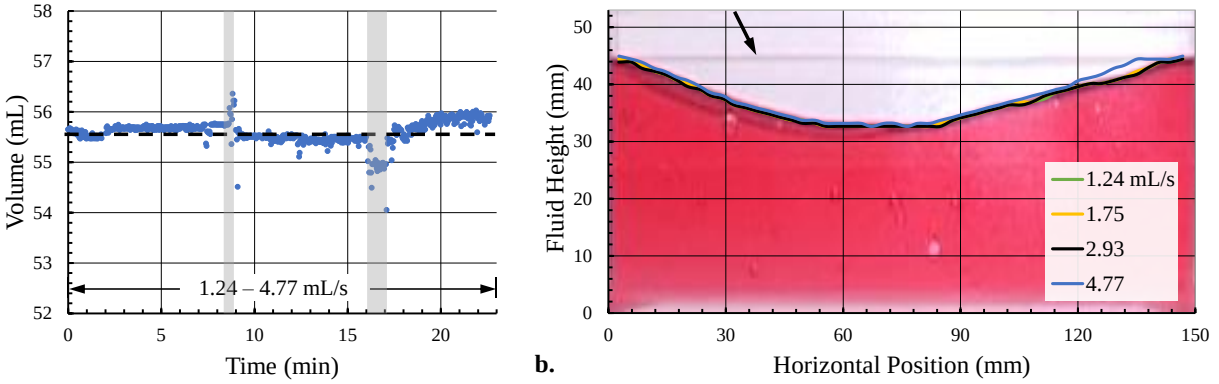

Figure 7. a. Approximately 23 min single Wedge channel flow for a ramp sweep in flow rate. Volume measurements are constant at 55.6 ± 0.4 mL apart from crew-induced disturbances during the run (indicated by grey boxes). b. Four free surface overlays on a representative (scaled) image of flow in a. demonstrating surface stability through the range of pump flow rates listed.

Figure 8 provides a selection of steady dynamic free surface configurations for demonstrations with a variety of plant root models. Stable conditions are established for up to approximately 15 min for single and multiple 'plants', varying fill levels, with and without bubbles, etc. Maximum flow rates for stable single channel flows were established to be 4.88 mL/s, with minimum flow rates ranging from 0.8-1.2 mL/s. The high rate was limited by the pump speed, while small variations in pump-head tubing tension (i.e., kit-to-kit variations) affected the lowest speed the pump could spin without stalling. Out-of-plane asymmetries in plant alignment led to local interface deflections and can lead to local depinning (ref. Figure 8b, c, and e), but were not observed to cause instability or degradation in channel performance. Entrance region recirculation zones as sketched in Figure 8 are readily observed at all flow rates tested and vary in intensity with plant root type, position, and flow rate. The high flow rate ranges produce inertial flows to the point Bernoulli suction is observed to pull down the fluid interface in the vicinity of the inlet stream. Despite the plant root obstructions in the Wedge channel tests, stable flows could be established in all situations depending on flow rate (a value < 0.8 mL/s, the minimum flow rate achievable by the onboard pump) with the maximum flow rate before reaching the gas ingestion limit varying as a function of fill level and root obstruction fraction. Pinning edges are also observed to serve as effective boundaries preventing upwards fluid migration. When over-filled or over-driven, as in the case of large roots (e.g., Figure 8f), the channel lid appears to function as a secondary pinning edge. Satellite droplets ejected by rupturing bubbles are also contained by the lid. A nonwetting material would rebound such droplets back to the channel liquid as well as provide a significantly improved pinning condition.

Figure 9 shows the typical operational cycle for a test run with a plant model. To insert the plant, the channel is partially drained, and the plant model is inserted, as seen in 9a. The channel is then refilled and run at a variety of fluid levels and pump speeds. Figure 9c-f demonstrate a variety of fill levels representative typical bubble injections, fluid accumulations, and liquid and gas bubble separations within the channel. At the conclusion of runs with a particular plant model, the channel is drained, and the plant model is gently though easily removed, as seen in 9g.-i. Of note here is that, despite the wetting nature of the roots, nearly all liquid remains attached to the channel as the plant model is removed, reducing the potential for free droplets during subsequent plant manipulations.

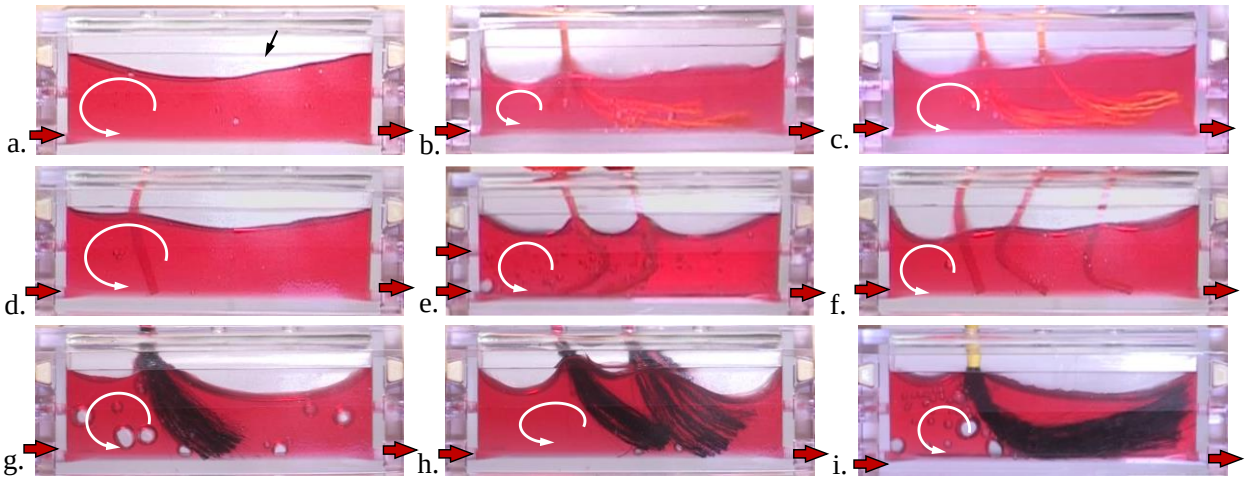

Figure 8. Variety of stable free surface configurations in Wedge channel at flow rates 1.64-1.85 mL/s. a. No plants (clip ref. 40), b.-c. nylon root plants (clip refs. 229, 234), d.-f. taproots (clip refs. 40, 65, 46), and g.-i. weave roots (clip refs. 81, 87, 126). Recirculation zones identified. Note local depinning in g and h where roots contact the wall of the container.

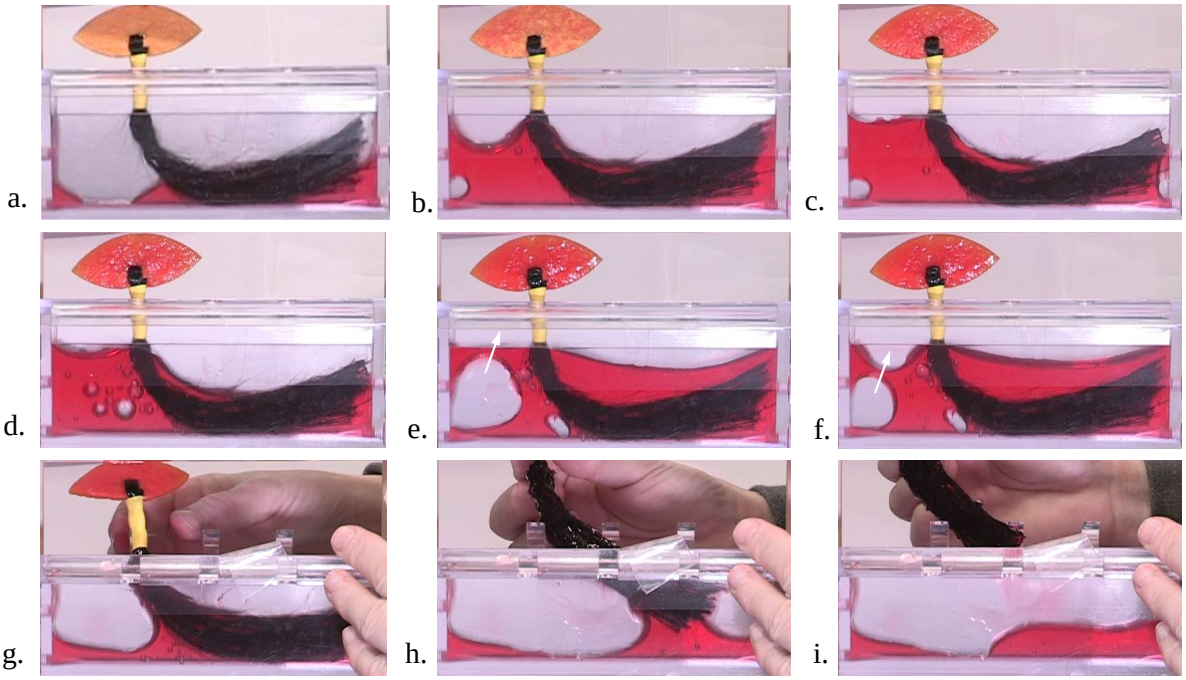

Figure 9. Select demonstrations of typical hydroponics activities (Wedge channel): a.-c. channel refill after new plant placement, d.-f. passive bubble separation (white arrow) in inlet region during steady bubbly flow operation (1.84 mL/s), and g.-i. 'no mess' plant removal. (Clip ref. #'s 111, 122, 129, 131)

C. Parallel Channel Flow: Limits of Operation

Stable parallel open capillary Wedge channel flows have been thoroughly demonstrated during previous space experiments with 2, 4, and 16 parallel channels.[6] With sufficient fill level, pinning, contact angle hysteresis, and limits on bubbly flow and flow rates, stable flows are achievable. Prior work has also demonstrated that manifold flow resistance is often greater than that of the open channels[10] and can play a significant role in flow balancing. PWM-Hydroponics 3 & 4 adds the complications of larger test cells, plants as obstacles, elevated flow rates, and a plethora of bubbles and bubble distributions in both channels and manifolds. Balanced flows are demonstrated as shown in

Figure 10a for the Wedge channel at 1.37 mL/s, where channel fill levels hold steady to measurement uncertainty during the 9 min test. Variations in tubing, manifold, and channel flow resistances can lead to small imbalances that result in a gradual shift of liquid from one channel to another. This phenomenon is illustrated and annotated in Figure 10b, where manual adjustments to the system are made to investigate the limits of stable parallel flow. The volume tracking data is noisy when obscured by the crew during the manual interventions. At the beginning of the run, both test cells are filled to approximately the same level and the pump is turned on. From the plot, a fluid shift from the lower to upper channel is observed. When the upper channel is nearly full, the pump is turned off and syringes were used to manually transfer fluid back to the lower channel. The pump is then turned on and though the instability is slowed it is not stopped. The instability is reversed when one upper channel inlet is closed and a second outlet is opened. This reduces the upper channel inflow and increases the upper channel outflow enough to reverse the instability, shifting liquid from upper to lower channel. Additional valve changes temper the transfer rate, but stable flow is not achieved for flow rate settings > 1.3 mL/s used for this test. The imbalances are easily controlled, but as this run shows, potentially difficult to maintain for a given channel arrangement above a flow rate threshold.

We also note that parallel flow instabilities can develop from previously stable flows. One notable example is of a 9 min stable parallel Cylinder channel flow which is disrupted when a gas bubble in the upper channel is dislodged from the outlet where the fitting screws into the channel (clip ref. 418). The occlusion had reduced the flow rate at the outlet of the channel, creating balanced flow between the channels until it became dislodged as the flowrate was increased, causing an immediate shift in fluid out of the upper channel. Thus, bubbles as well as tubing, fittings, manifolds, and valve asymmetries can all lead to premature parallel flow instability.

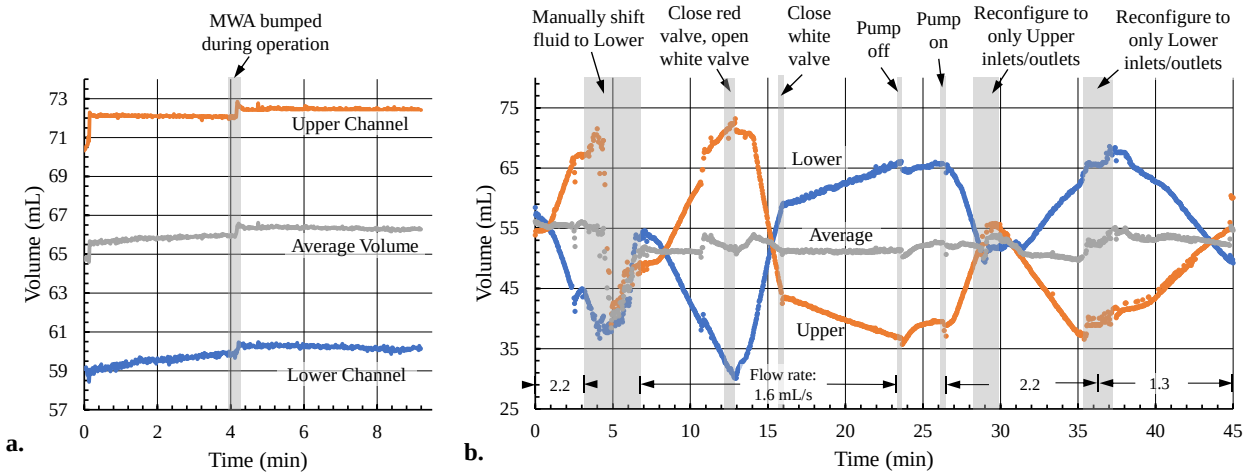

Figure 10. a. Effectively constant channel volumes during long duration stable parallel flow in Wedge channel (1.37 mL/s, clip ref. 220). b. Transient upper and lower Wedge channel volume shifts during parallel flow instability tests. Average volume is shown in gray. Manual efforts to balance the system are noted above (Ref. Figure 3 for valve color assignments, clip refs. 21-28).

Figure 11. Parallel Wedge channel flows images from runs in Figure 10. a. stable configuration corresponding to Figure 10a, *t* = 5:00. b. Channel fill states after a fluid shift from lower to upper channel. Corresponds to Figure 10b, *t* = 12:50. c. Fluid shift in progress from upper to lower channel shortly before configuration change. Corresponds to Figure 10b, *t* = 36:30.

From previous experiments, for low enough flow rates, we know that strong contact line pinning edges and significant contact angle hysteresis will eventually stabilize these second order shifting flows – the liquid rises until it pins in a stabilized though unevenly distributed flow. At least 11 stable parallel flow conditions were established in these demonstrations. At least 58 unstable parallel flow conditions were established and triggered in part by large channels, plant model obstructions and asymmetries, pinch valve variability, partially occluding wall-bound bubbles, manifold asymmetries, elevated flow rates, and a pinning edge design flaw. [We note here that the pinning edge was intended to frame the perimeter of the channel. Unfortunately, an inspection oversight missed that the printed pinning edges only occur along parallel lines in the flow direction, and not in the cross-flow direction at the entrances and exits to the channels. As only briefly addressed herein, this fact did not prevent any of the demonstration objectives from being achieved. It did, however, weaken free surface pinning for certain tests including the parallel flow instability tests. Fortunately for the investigator team, the crew was able to quickly and cleanly recover from at least 9 de-wetting or overflow events that partially covered the channel lids. In such instances, the crew withdrew excess fluid from the wetted channel, opened the lid, dabbed the lid and pinning edges with a towelette, replaced the lid, and quickly returned to the procedures. We note that though stable flows were readily achieved by the channel designs tested, stability would have been markedly improved had the pinning edge of the channel been continuous and made of a non-wetting material.]

D. Serial Channel Flow

A serial Wedge channel flow was only briefly demonstrated using the serial bypass line (ref. Figure 3 for location), where the flow proceeded through the upper channel, bypass line, and then through the lower channel. Such tests have proven successful for smaller, slower systems such as those described in References 6 and 11. However, in the flow rate ranges of PWM-Hydroponics (>0.9 mL/s), though serial flow could be observed, flow rate conditions could not be established to avoid the rapid shift of liquid from the downstream to the upstream channel, typically resulting in upstream channel overflow within 1 min of run start.

E. Further Limits of Operation

A variety of additional instability mechanisms were pursued as a means to identify the practical limits of operation of the low-g hydroponics system. These include, but are not limited to, any combinations of flow instability due to gas ingestion and liquid depinning leading to the pinning edge overflowing (the ‘de-pinning’ limit). In all cases demonstrated, the liquid remained contained by the channel lid, and complete recovery of the system was possible with simple crew actions. For example, three instabilities are shown in Figure 12 highlighting the gas ingestion limit, the de-pinning limit, and the potential ill-effects gas bubble accumulation (Cylinder channel only). As shown in Figure 12a, gas ingestion occurs in a single Wedge channel flow when the flow at the outlet exceeds the capillary pumping limit through the roots resulting in a series of gas bubbles ingested into the channel exit, which travel through the system and are re-injected into channel. Of the myriad bubbles flowing through the channel, one such bubble lodges in the root bundle increasing the capillary flow resistance causing a rapid reduction in pumping capacity of the system and gas ingestions without the pump flow rate changing. This run was manually stopped at this point, however in many cases the build-up of liquid at the channel inlet reduces the flow resistance and the flow recovers from bubble ingestion, gradually expelling the gas bubbles through coalescence and separation in the Wedge.

In Figure 12b, bubbles coalesce with a large bubble pinned at the inlet of the Wedge channel and accumulate along the plant roots. The pinned bubble grows both by the coalescence of bubbles flowing into the channel and bubbles caught in the inertial recirculation zone in the channel inlet region. The combination of the large root mass with pinned and wall-bound bubbles further reduces the size of the recirculation zone. The merged bubbles form several large bubbles, increasing the overall system volume until the fluid de-pins from the pinning edge. Once free from the pinning edge, bulk fluid rapidly rises (~ 5 sec) and fills the interior corner of the bottom of the lid, necessitating a pause in experiments for a partial drain and recovery.

In Figure 12c, a Cylinder channel with plants illustrates how the cylindrical cross section, when combined with plant root obstructions, can trap bubbles in the rounded portion of the channel. These bubbles coalesce and grow until they completely occlude the cylindrical portion of the channel leading to film rupture across the partially wetting solid surface. Immediately after the liquid surface ruptured, the outlet begins to ingest bubbles as a result of the sudden loss of liquid supply. Accumulated liquid in the system recovers a continuous liquid free surface, however, the large merged bubbles continue to circulate through the system, reaching the inlet, and the process repeats. Large bubbles in the cylinder can also work their way underneath the root bundle, forcing the roots upward with continued bubble growth—a phenomena potentially unfavorable to real plants. Further increases in coalesced bubble volume can lead

to its ingestion with the possibility of subsequent de-pinning and plant root deflections. These phenomena appear only to occur in the Cylinder channel.

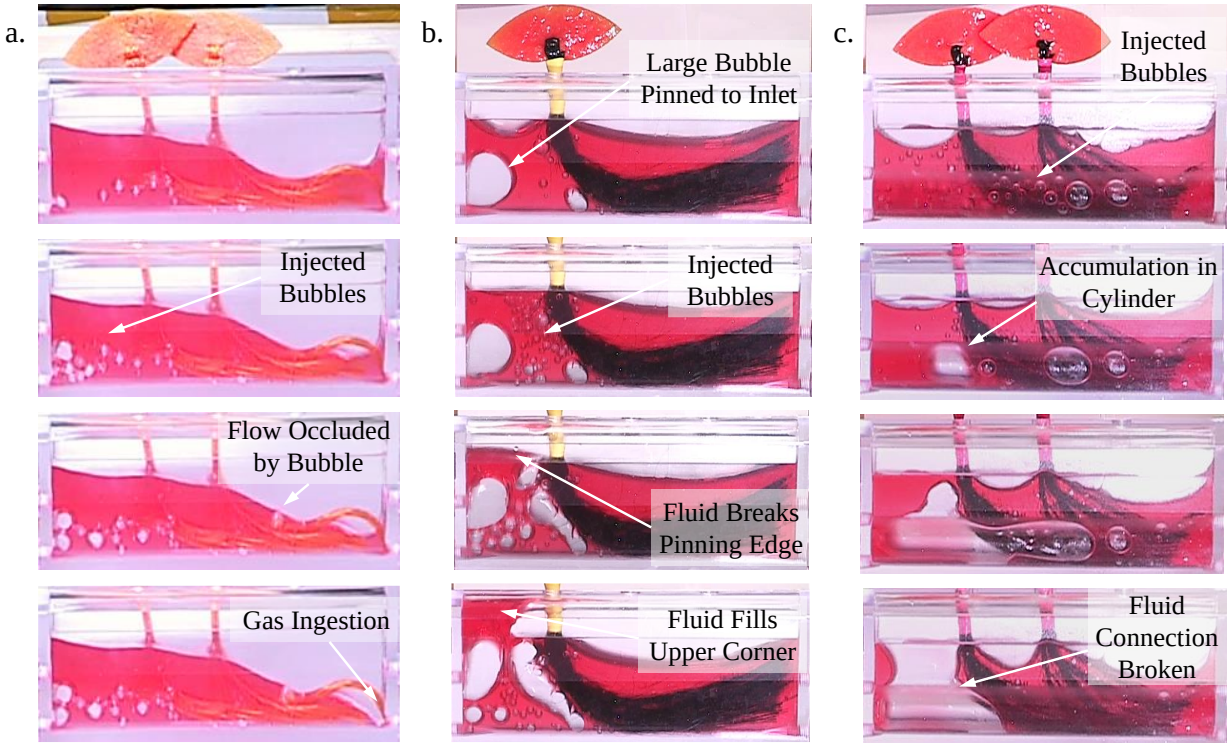

Figure 12. Specific flow instability demonstrations: a. ingestion limit in Wedge channel with nearly root plugged channel (1.11 mL/s, clip ref. 249), b. de-pinning limit in Wedge channel due to inlet bubble coalescence leading to depinning (1.82 mL/s, clip ref. 130), and c. bubble coalescence in Cylinder channel inlet leading to break-up and disconnection between inlet and inlet and outlet fluid bodies (1.67 mL/s, clip refs. 164-170).

F. Impact of Bubbles and Bubble Separation

Any plant watering system for application in space must account for the presence of bubbles whether produced inadvertently by degassing or biochemistry or purposely by bubble ingestion or direct injection for liquid aeration. The PWM-Hydroponics 3 & 4 experiments created bubbles purposefully by forced ingestion at the channel exits as well as by direct injection using the gas syringe. Bubble distributions and behavior are observed as noted in Figures 8, 9, 12 and 13. At least 129 tests were conducted towards this end. In general, we find that single Wedge channel flows are insensitive to the presence of bubbles. Tiny bubbles simply circulate through the loop, potentially coalescing in the entrance region recirculation zone, while larger bubbles become wall-bound, merge together, rise in the channel, coalesce with the free surface, and leave the flow (e.g., clip refs. 130-134).

The coalescence, migration and merging were investigated with a wide variety of single and multi-bubble injections. Up to 20 mL of air could be injected at a time into the circulating liquid using the gas syringe. Several examples of the behavior and gradual elimination of bubbles resulting from 10 mL injections are shown in Figure 13 for three different fill levels. Figure 13a. and b. demonstrate the initial cluster of small bubbles, the coalescence over 30 seconds into a few larger bubbles, the migration of these bubbles upwards and the eventual mergers with the free surface. Figure 13c. displays similar bubble eliminations while also highlighting the ability of the system to recover from an odd liquid configuration resulted from a previous large gas bubble merger on the lefthand side of the container.

Because inadvertent bubbles have the potential to completely destabilize such capillary flows, and because plants in low-g environments often suffer from hypoxic conditions, the team dedicated over 7 hours of experiment time to investigating bubbly flows in both Wedge and Cylinder channels. The drawbacks encountered with the Cylinder design have been discussed previously, however for the Wedge design, the channel itself is found to be self-clearing in most scenarios. This reduces the requirement for a bubble-free prime, any need to limit liquid off-gassing, or be concerned with gases produced by biochemical reactions within the plants.

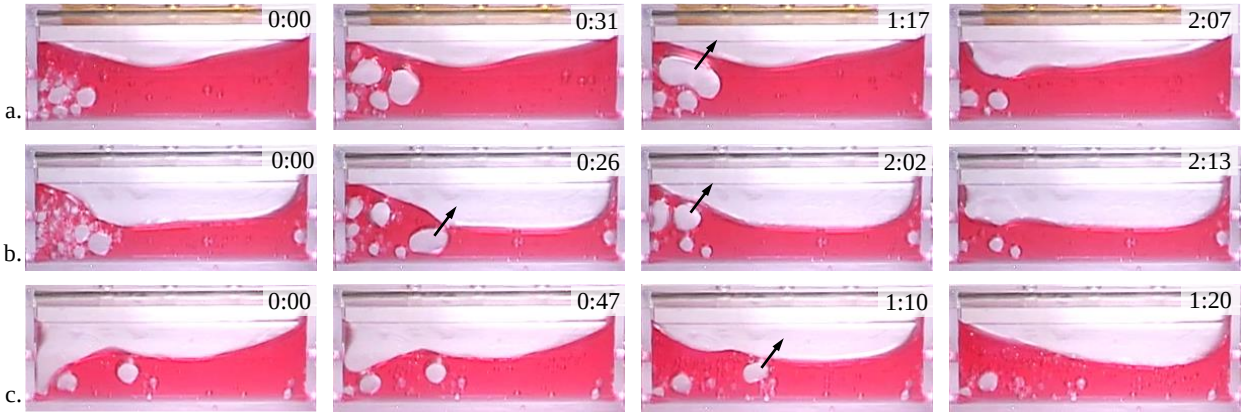

Figure 13. Passive bubble separation (black arrows) in Wedge channel after 10 mL gas syringe injections: a. 39 mL fill at 0.9 mL/s (clip ref. 273), b. 25 mL fill at 1.33 mL/s (clip ref. 281), and c. 31.5 mL fill at 2.52 mL/s (clip ref. 289). All flows eventually become 'bubble free,' however larger bubbles in slower flows tend to become wall-bound, slowing their progress towards merging with the free surface.

One method to improve gas separation efficiency is to introduce the bubbles closer to the channel free surface. This is demonstrated by replacing the upstream wye fittings with 'bubble diverters' that serve to divert most bubbles to the upper inlet of the channel where they concentrate, merge, coalesce, and leave through the free surface. To provide the desired control for such tests, trains of known bubble volume and number were created by turning off the pump, injecting the chosen gas volume, toggling the pump, injecting again the chosen volume, and so on until a train of known bubble volume and number was created. The pump setting was then adjusted and pump turned back on. In this way, the bubble diverters separation efficiency as a function of flowrate and bubble size can be accurately quantified, however at this time analysis of these data are not complete.

Figure 14b. and c. show images of the two bubble diverter designs tested, while Figure 14d. and e. provide representative examples of phase separation performance, where gas volume separation efficiencies are readily > 99%. For highly regulated bubble flows, efficiencies can approach 100.0%. With bubble diverter performance in hand and with knowledge of the ingestion limit for the channel, the system can be over-driven while maintaining a stable bubble ingestion rate at the channel exit (clip ref. 367). These bubbles aerate the liquid as they pass through the loop, only to be diverted and separated in the entrance region of the channel upstream of the first plant obstruction. Significant increases in Technology Readiness Level (i.e., from TRL 5 to approximately 7) are anticipated for this passive aeration/bubble diversion approach for future PWM-Hydroponics 5 & 6 work.

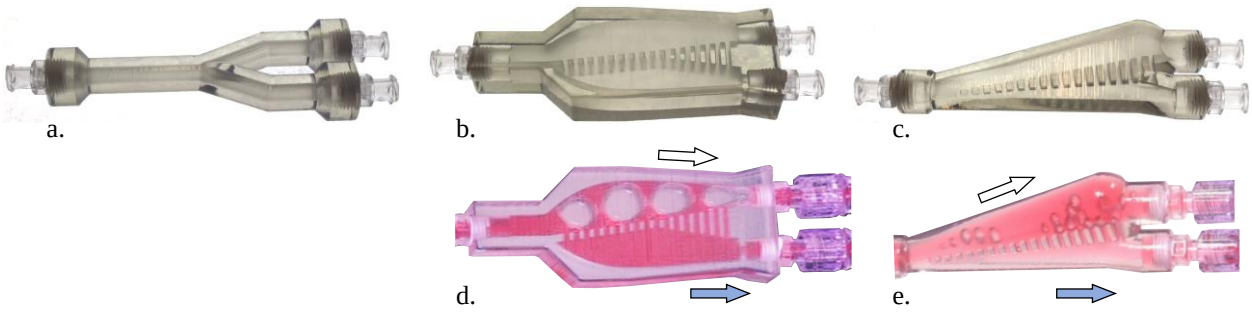

Figure 14. Upstream fitting with characteristic volumetric separation/diversion efficiency for bubbles tested (in %): a. non-diverting wye (50%), b. bubble diverter I (98%) and c. bubble diverter II (> 99%). Flight images of performance in d. and e.

G. Passive Liquid Reservoir Demonstration

Over 90 min were spent demonstrating the passive infill capabilities of the Fluid Reservoir with in-fill rates in the range 0.0235 ± 0.0015 mL/min demonstrated during a 36 min run shown in Figure 15a, which plots the decreasing

volume remaining in the reservoir. Referring to Figure 3, opening the valves at either end of the reservoir (Fluid reservoir valve and breather valve), the under-pressure of the loop naturally drew liquid from the reservoir. A Rayon felt wick within the reservoir helped to maintain capillary connection between the reservoir and loop. Pressure differences between the reservoir and loop could be adjusted via a variable pinch valve at the base of the reservoir. Demonstrations of this passive 'evapotranspiration make-up flow' suggest that, with patience, the reservoir valve might be adjusted to match desired set-points such as out-flow rate (maintaining evapotranspiration rate), or out-flow pressure (maintaining constant fill level). Fine-tuning the fluid reservoir parameters will become more important as longer duration runs are pursued in future flight experiments.

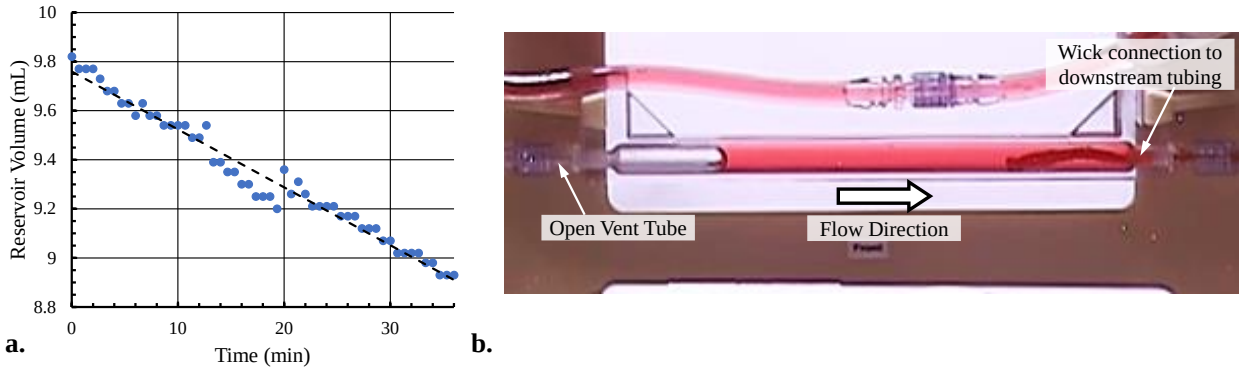

Figure 15. a. Plot of the remaining volume in the passive reservoir during a 36 min long-duration run. The dashed line is a linear fit with an average drain rate of 23.6 mm^3/min. b. Detailed depiction of the meniscus in the passive reservoir during use. Direction of outflow indicated with large arrow. The tube on the left is open to cabin air for pressure relief, while dark object in the fluid is a felt wick connecting to the downstream tubing.

V. Conclusion

The PWM-Hydroponics 3 & 4 technology demonstration experiments provide a sizable database from which to assess and develop increasingly practical low-g hydroponics plant watering systems that operate similarly to terrestrial systems. In low-g environments, the role of gravity is replaced by the combined effects of surface tension, wetting, and channel geometry. We find that an open wedge channel geometry can achieve stable flow conditions of up to our maximum flow rate of 5 mL/s, for a 76 mL, 150 mm long channel with a variety of synthetic plant types and number installed. The overall system is relatively insensitive to the presence of bubbles, a property which may be exploited to manage bubbles purposefully and passively for liquid aeration. Single and parallel channel flow configurations are demonstrated as well as the limits of operation regarding channel size, flow rates, fill levels, bubble throughput, etc. Stable system operation is expected below these newly established limits. Operating above these limits can lead to significant exit bubble ingestion, entrance over-filling, and liquid de-pinning. When excursions occur, these events are neatly contained by the zero-level-of-containment channels and the attached lids, allowing for simple often passive recovery and re-establishment of stable steady or stable steady periodic behavior. If operating near channel flow limits, bubble ingestion and liquid de-pinning are readily prevented via demonstrated methods such as the use of bubble separators and passive fluid re-fill reservoirs with simple manual or automatable interventions or controls.

Practical demonstrations of system start-up, steady operation, response to excursions, physical perturbations, plant size and number, plant placement and removal, and system shutdown and restart are all catalogued and hyperlinked in an archive to be made publicly available on the NASA Physical Science Informatics database (https://psi.nasa.gov). Over 430 individual test cases are currently catalogued. The archive may be used to acquire specific data as well to become familiarized with the rare long-duration low-g footage of the highly variable behavior of aqueous capillary solutions in irregular channels. Presently planned follow-on demonstrations via PWM-Hydroponics 5 & 6 aboard ISS in 2023 will focus on the refinement of fluidic elements, long duration steady states, the possibility of real plants with real nutrient solution, automation, and passive and active controls. The salient lessons learned from PWM 3 & 4 that will be invaluable to advanced system design include:

- Open channel visco-inertial-capillary flows are highly stable in single channels for wide range of fill levels
- Robust pinning edges and high contact angle hysteresis enhances fluid stability
- Parallel channel flows are stable below a certain flow rate threshold

- At higher flow rates, parallel flows can become unstable due to differences in resistances caused by tubing, fittings, valves, manifolds, plant obstructions, and bubble movement. Over time, small flow resistance imbalances can lead to large asymmetric shifts in fluid distribution which are easily prevented or controlled
- System prime, start-up, shut-down, restart, etc. do not pose significant challenges to the system due to the passive two-phase flow separating nature of the Wedge channel geometry
- Current design guides are effective at predicting target performance and flow stability to excursions and physical perturbations.

A more detailed review of the PWM 3 & 4 flight experiments is expected shortly.[12]

Acknowledgements

This work was supported in part through NASA Cooperative Agreement 80NSSC18K0436 and NASA SBIR PhI 80NSSC19C0252, with early insights regarding plant growth metrics provided by NASA KSC personnel. The authors are deeply grateful for the efficient, insightful, and enjoyable support of the ISS cadre and Crew: US astronauts Michael Hopkins, Shane Kimbrough, Megan McArthur, Kate Rubins, Mark Vande Hei (first commercial crew), and French ESA astronaut Thomas Pesquet. We also thank Rihana Mungin for plant model development and CSS and Inc. and ECI Inc. for hardware fabrication and flight qualification.

References

[1]Concus, P., & Finn, R, (1969) "On the behavior of a capillary surface in a wedge." *Proceedings of the National Academy of Sciences of the United States of America*, 63.2:292.

[2]Romero, L.A. & Yost, F.G., (1996) "Flow in an open channel capillary." *Journal of Fluid Mechanics*, 322: 109-129.

[3]Weislogel, M.M, Baker, A. & Jenson, R.M., (2011) "Quasi-steady capillarity-driven flows in slender containers with interior edges." *Journal of Fluid Mechanics*, 685: 271-305.

[4]Weislogel, M.M., Jenson, R., Chen, Y., Collicott, S.H., Klatte, J. & Dreyer, M., (2009) "The capillary flow experiments aboard the International Space Station: Status." *Acta Astronautica* 65(5-6): 861-869.

[5]Conrath, M., Canfield, P. J., Bronowicki, P. M., Dreyer, M. E., Weislogel, M. M., & Grah, A. (2013) "Capillary channel flow experiments aboard the International Space Station." *Physical Review E.* 88(6): 063009.

[6]Weislogel, M.M., & Jensen, R.M., (2018) "Final Report: Capillary Structures for Exploration Life Support (CSELS) Flight Experiment." IRPI LLC Contract No. NNX16CJ54P, 2018.

[6]Viestenz , K.J., Jenson , R.M., Weislogel, M.M., Sargusingh, M.J., Capillary Structures for Exploration Life Support Payload Experiment, 48th Int. Conf. on Environmental Systems, ICES-2018-241, 11 pages, 8-12 July 2018, Albuquerque, New Mexico.

[7]Torres, L.J., Jenson R., and Weislogel, M., (2020) "Capillary Hydroponic Plant Watering System for Spacecraft." *50th International Conference on Environmental Systems*, Lisbon, No. 172.

[8]Mungin, R., Weislogel, M., Hatch, T., McQuillen, J., (2019) "Omni-gravity Hydroponics for Space Exploration," *49th International Conference on Environmental Systems*, Boston, No. 242.

[9]Weislogel, M.M., & Jensen, R.M., (2017) "CSELS Sorbent Pump Characterization" IRPI LLC Contract No. NNX16CJ54P.

[10]Mohler, S. and M. Weislogel. "A Thin Film Liquid Sorbent Reactor for CO2 Scrubbing Aboard Spacecraft." 2020 International Conference on Environmental Systems, 2020.

[11]Hatch, T., M. Weislogel, R. Mungin, J. McQuillen, Plant Water Management in Microgravity, 50th International Conference on Environmental Systems, ICES-2020-28, 9 pages, Lisbon, 12-16 July, 2020.

[12]Wasserman, M.B., The Plant Water Management Experiments, MSME Thesis, Portland State University, 2022 (to appear).